Improved and Interpretable Solar Flare Predictions with Spatial and Topological Features of the Polarity-Inversion-Line Masked Magnetograms[1]

Hu Sun [1]

Ward Manchester[2], Yang Chen[1]

[1]Department of Statistics, University of Michigan, Ann Arbor

[2]Department of Climate and Space Sciences and Engineering, University of Michigan, Ann Arbor

Sept 20, 2021

[1]Our submitted manuscript can be viewed at https://www.essoar.org/doi/abs/10.1002/essoar.10507540.1

Overview

Flare Prediction with HMI Magnetograms

- Bobra, Sun, et al. (2014) introduced the Space-weather HMI Active Region Patch (SHARP) parameters, which are derived from the magnetograms of the HMI/SDO images and have been used by a lot of the solar flare prediction models in recent years (e.g. Bobra and Couvidat, 2015; Florios et al., 2018; Chen et al., 2019; Camporeale, 2019; Jiao et al., 2020).

Flare Prediction with HMI Magnetograms

- Bobra, Sun, et al. (2014) introduced the Space-weather HMI Active Region Patch (SHARP) parameters, which are derived from the magnetograms of the HMI/SDO images and have been used by a lot of the solar flare prediction models in recent years (e.g. Bobra and Couvidat, 2015; Florios et al., 2018; Chen et al., 2019; Camporeale, 2019; Jiao et al., 2020).
- There are efforts of using the deep neural network methods which directly takes the HMI/SDO magnetogram images to predict solar eruptions (e.g. the Long Short Term Memory network adopted by Chen et al. (2019) and Liu et al. (2019)).

Flare Prediction with HMI Magnetograms

- Bobra, Sun, et al. (2014) introduced the Space-weather HMI Active Region Patch (SHARP) parameters, which are derived from the magnetograms of the HMI/SDO images and have been used by a lot of the solar flare prediction models in recent years (e.g. Bobra and Couvidat, 2015; Florios et al., 2018; Chen et al., 2019; Camporeale, 2019; Jiao et al., 2020).
- There are efforts of using the deep neural network methods which directly takes the HMI/SDO magnetogram images to predict solar eruptions (e.g. the Long Short Term Memory network adopted by Chen et al. (2019) and Liu et al. (2019)).
- Recent efforts (Deshmukh, Berger, Bradley, et al., 2020; Deshmukh, Berger, Meiss, et al., 2020) leverage the shape information contained in HMI magnetograms to construct interpretable and predictive new parameters for flare prediction.

Highlights of Our Work

1. Expand the feature set derived from the HMI magnetograms for flare prediction using tools from both *topological data analysis* and *spatial statistics*.

Highlights of Our Work

1. Expand the feature set derived from the HMI magnetograms for flare prediction using tools from both *topological data analysis* and *spatial statistics*.
2. Derive features not only from the PIL-masked HMI magnetograms but also from SHARP parameter masks.

Highlights of Our Work

1. Expand the feature set derived from the HMI magnetograms for flare prediction using tools from both *topological data analysis* and *spatial statistics*.
2. Derive features not only from the PIL-masked HMI magnetograms but also from SHARP parameter masks.
3. Marginally but steadily improved the skill score of the classification model of strong vs. weak solar flares.

Dataset

- We use the Geostationary Operational Environmental Satellites (GOES) flare list spanning 2010/12 - 2018/06 for collecting flare events, leading to 399 M/X class flares and 1,972 B class flares coming from 487 HARP regions.

Dataset

- We use the Geostationary Operational Environmental Satellites (GOES) flare list spanning 2010/12 - 2018/06 for collecting flare events, leading to 399 M/X class flares and 1,972 B class flares coming from 487 HARP regions.
- For each flare, we collect its corresponding high-resolution HMI magnetogram data from the JSOC at 4 time points: 1, 6, 12, 24 hours prior to the peak flux.

Dataset

- We use the Geostationary Operational Environmental Satellites (GOES) flare list spanning 2010/12 - 2018/06 for collecting flare events, leading to 399 M/X class flares and 1,972 B class flares coming from 487 HARP regions.
- For each flare, we collect its corresponding high-resolution HMI magnetogram data from the JSOC at 4 time points: 1, 6, 12, 24 hours prior to the peak flux.
- For each flare at any of four time points, raw data of the B_r, B_p, B_t components of the magnetic field are collected.

Derive SHARP Parameter Maps

- We derive features from the B_r component of the magnetic field but also from other secondary maps derived from the B_r, B_p, B_t components, which we call *SHARP parameter maps*.

Derive SHARP Parameter Maps

Channel	Formula	Unit
Br	$\mathbf{B}_z$	G
GAM	$\arctan\left(\frac{\mathbf{B}_h}{\mathbf{B}_z}\right)$	Degree
GBT	$\sqrt{\left(\frac{\partial \mathbf{B}}{\partial x}\right)^2+\left(\frac{\partial \mathbf{B}}{\partial y}\right)^2}$	G$\times$ Mm^{-1}
GBH	$\sqrt{\left(\frac{\partial \mathbf{B}_h}{\partial x}\right)^2+\left(\frac{\partial \mathbf{B}_h}{\partial y}\right)^2}$	G$\times$ Mm^{-1}
GBZ	$\sqrt{\left(\frac{\partial \mathbf{B}_z}{\partial x}\right)^2+\left(\frac{\partial \mathbf{B}_z}{\partial y}\right)^2}$	G$\times$ Mm^{-1}
USJZ	$\lvert\left(\frac{\partial \mathbf{B}_y}{\partial x}-\frac{\partial \mathbf{B}_x}{\partial y}\right)\rvert$	A
USJH	$\lvert \boldsymbol{J}_z \times \mathbf{B}_z \rvert$	G^2 m $^{-1}$
POT	$\left((\mathbf{B}_x-\mathbf{B}_x^{POT})^2+(\mathbf{B}_y-\mathbf{B}_y^{POT})^2\right)$	erg cm^{-3}
SHR	$\arccos\left(\frac{\mathbf{B}_x^{POT}\times\mathbf{B}_x+\mathbf{B}_y^{POT}\times\mathbf{B}_y+\mathbf{B}_z^2}{\sqrt{\mathbf{B}_x^{POT\,2}+\mathbf{B}_y^{POT\,2}+\mathbf{B}_z^2}\sqrt{\mathbf{B}_x^2+\mathbf{B}_y^2+\mathbf{B}_z^2}}\right)$	Degree

Table 1. SHARP parameter mask, formula applied to every pixel of the HMI magnetogram. Here, $\mathbf{B}_x, \mathbf{B}_y, \mathbf{B}_z$ are the x, y, z components of the magnetic field and $\mathbf{B}_x^{POT}, \mathbf{B}_y^{POT}$ the potential field components respectively. Detailed definition of the parameters can be found in Table 3 of Bobra et al. (2014).

Derive the Polarity Inversion Line (PIL)

- We focus specifically on the area adjacent to the polarity inversion line (PIL) by constructing the PIL mask.

Derive the Polarity Inversion Line (PIL)

(a) Br, 1 hour before M flare

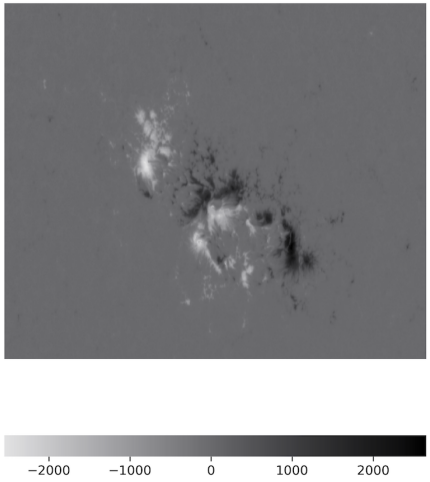

(b) PIL mask

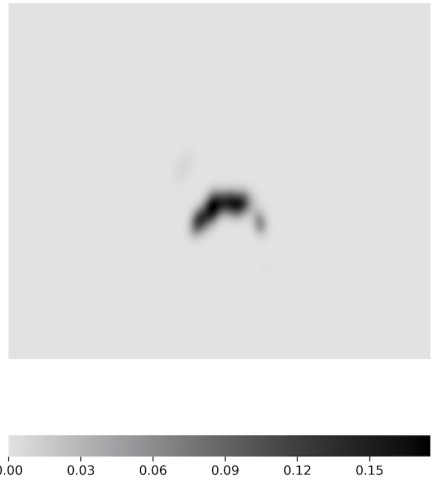

(c) |Br| > 200 G & PIL mask

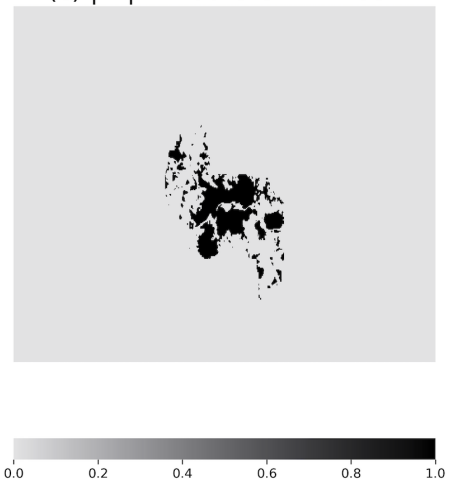

(d) Br, 1 hour before B flare

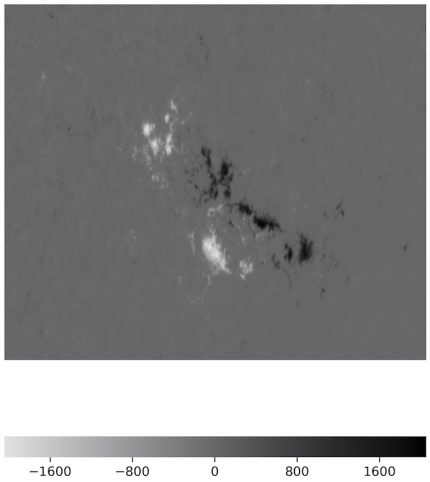

(e) PIL mask

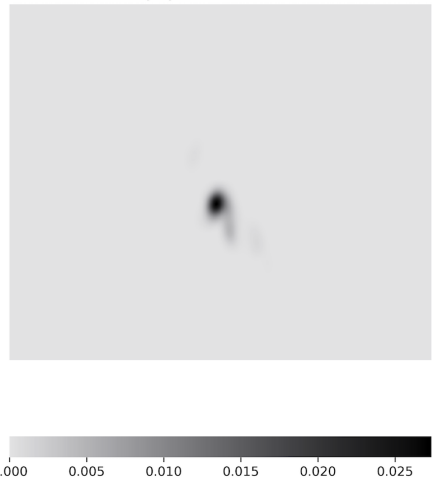

(f) |Br| > 200 G & PIL mask

Topological Feature: Betti Numbers

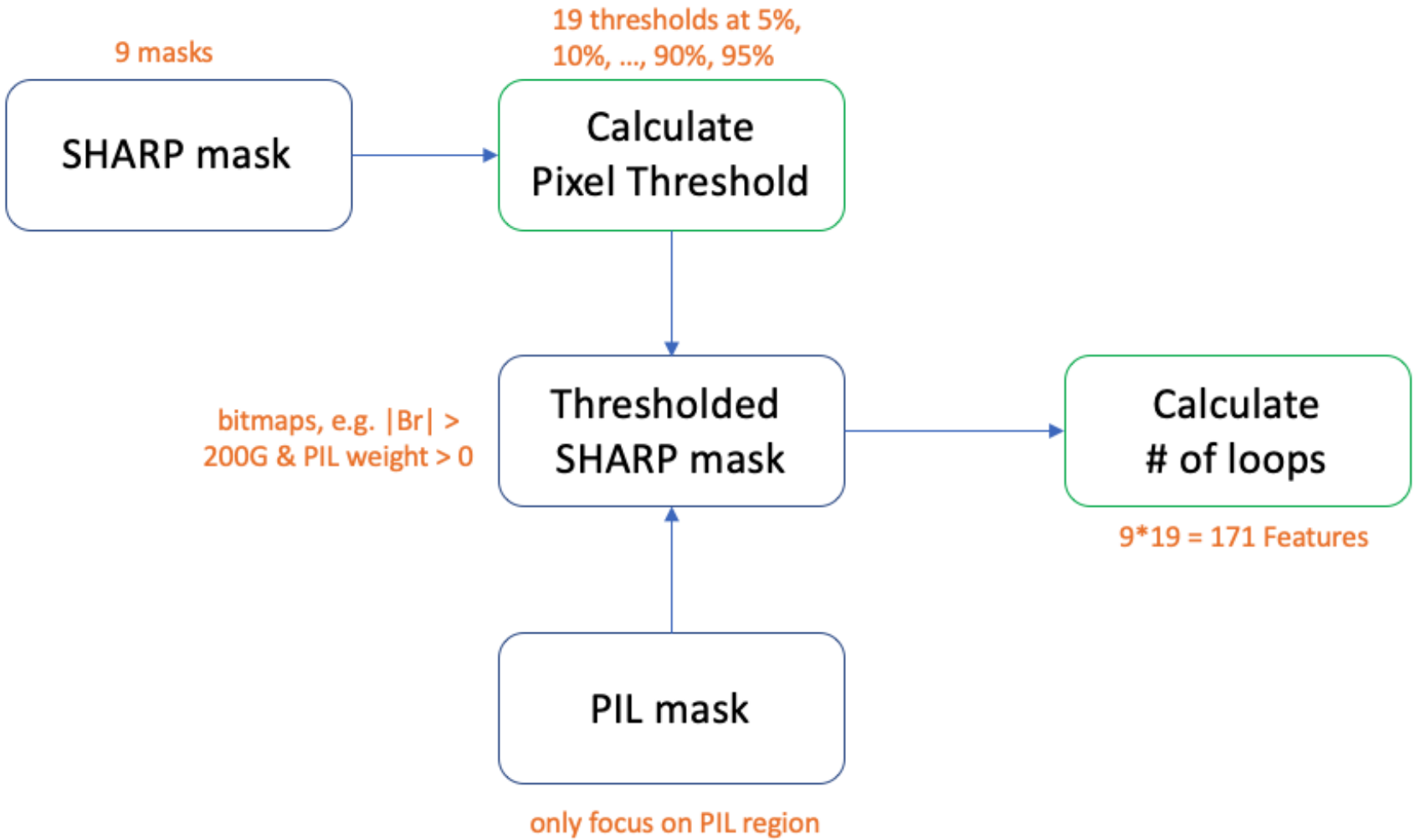

Figure: Feature Engineering Pipeline of Topological Features

Topological Feature: Betti Numbers

(a) Low Threshold

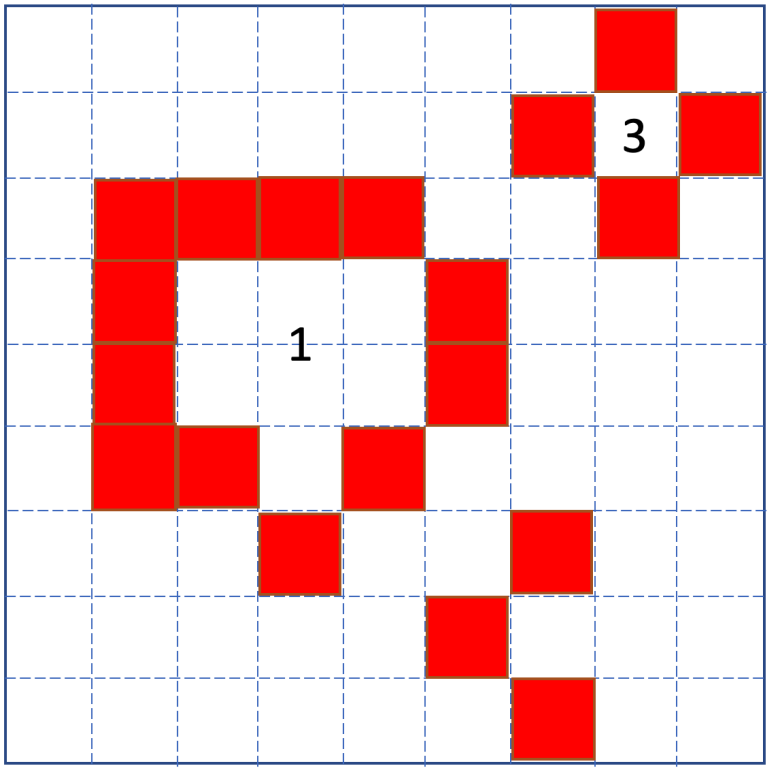

(b) High Threshold

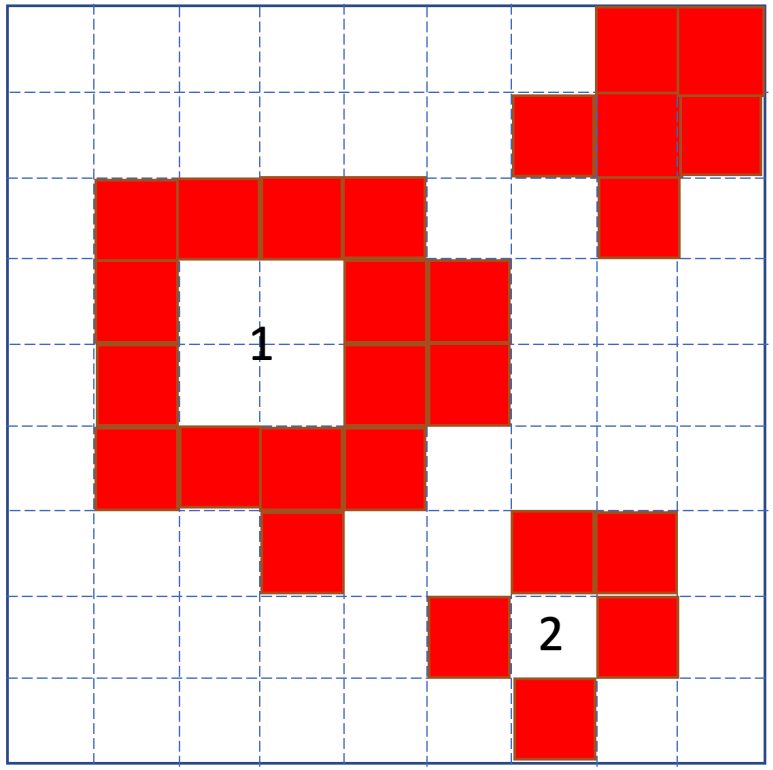

Figure: What is a loop?

Spatial Feature I: Ripley's K Function

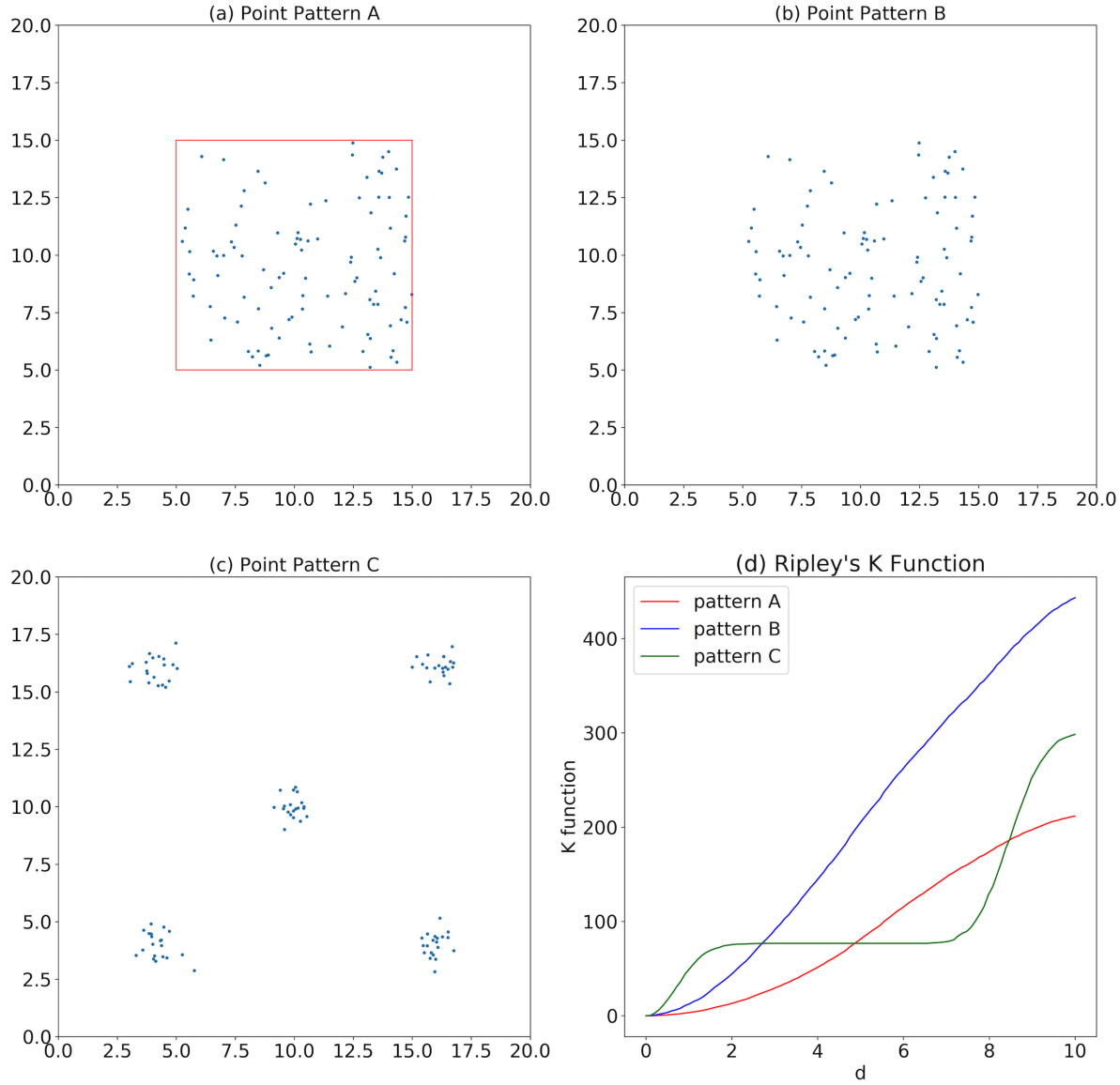

Spatial Feature I: Ripley's K Function

- For the thresholded B_r mask, we randomly pick 500 pixels, with sampling probability proportional to $|B_r|$, to construct a point cloud. Each picked pixel has a pair of (x, y) pixel coordinates in the 2D pixel grid.
- Ripley's K function:

$$L(d) = \sqrt{\frac{A \sum_{i=1}^{n} \sum_{j=1, j \neq i}^{n} k_{i,j}}{\pi n(n-1)}},$$

where $k_{i,j} = 1$ if the i-th and j-th pixel are within distance d, and $n = 500$ in our case. A is the area size and is defined as the number of PIL pixels in our study.

Spatial Feature I: Ripley's K Function

- For the thresholded B_r mask, we randomly pick 500 pixels, with sampling probability proportional to $|B_r|$, to construct a point cloud. Each picked pixel has a pair of (x, y) pixel coordinates in the 2D pixel grid.
- Ripley's K function:

$$L(d) = \sqrt{\frac{A \sum_{i=1}^{n} \sum_{j=1, j \neq i}^{n} k_{i,j}}{\pi n(n-1)}},$$

where $k_{i,j} = 1$ if the i-th and j-th pixel are within distance d, and $n = 500$ in our case. A is the area size and is defined as the number of PIL pixels in our study.

Spatial Feature I: Ripley's K Function

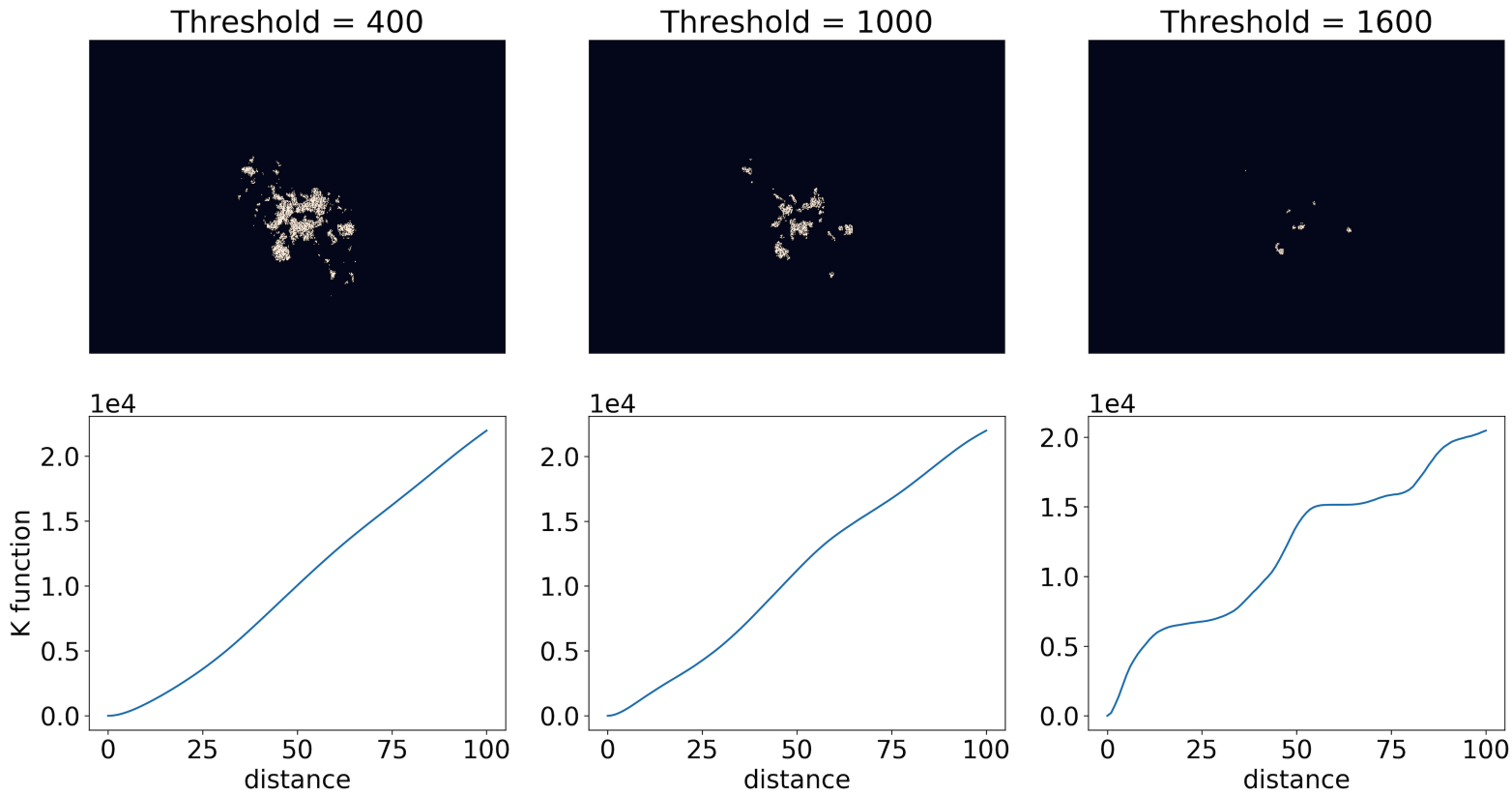

Figure: Point cloud and the corresponding Ripley's K function for the B_r mask collected from HARP 377, 1 hour before the M flare peaked at 2011.02.13 17:38. The top row includes 3 point clouds generated by 3 thresholds at 400G, 1000G, 1600G. The bottom row shows the 3 corresponding Ripley's K functions.

Spatial Feature II: Variogram

- With the same point cloud as in Ripley's K function calculation, the Variogram is:

$$\gamma(d) = \frac{1}{2}\mathrm{Var}[z(\boldsymbol{s}_i) - z(\boldsymbol{s}_j)], \tag{1}$$

  where $\boldsymbol{s}_i = (x_i, y_i), \boldsymbol{s}_j = (x_j, y_j)$ are two arbitrary points in the point cloud that has a Euclidean distance d in-between, and Var denotes the variance of a random variable. And $z(.)$ yields the B_r value at a pixel.
- In practice, it is hard to find multiple pairs of pixels separated exactly by distance d. Pairs of pixels will be put into disjoint bins of Euclidean distance for estimating the Variogram.
- Variogram is measuring the variation of B_r at two spatial locations separated by an arbitrary distance d.

Spatial Feature II: Variogram

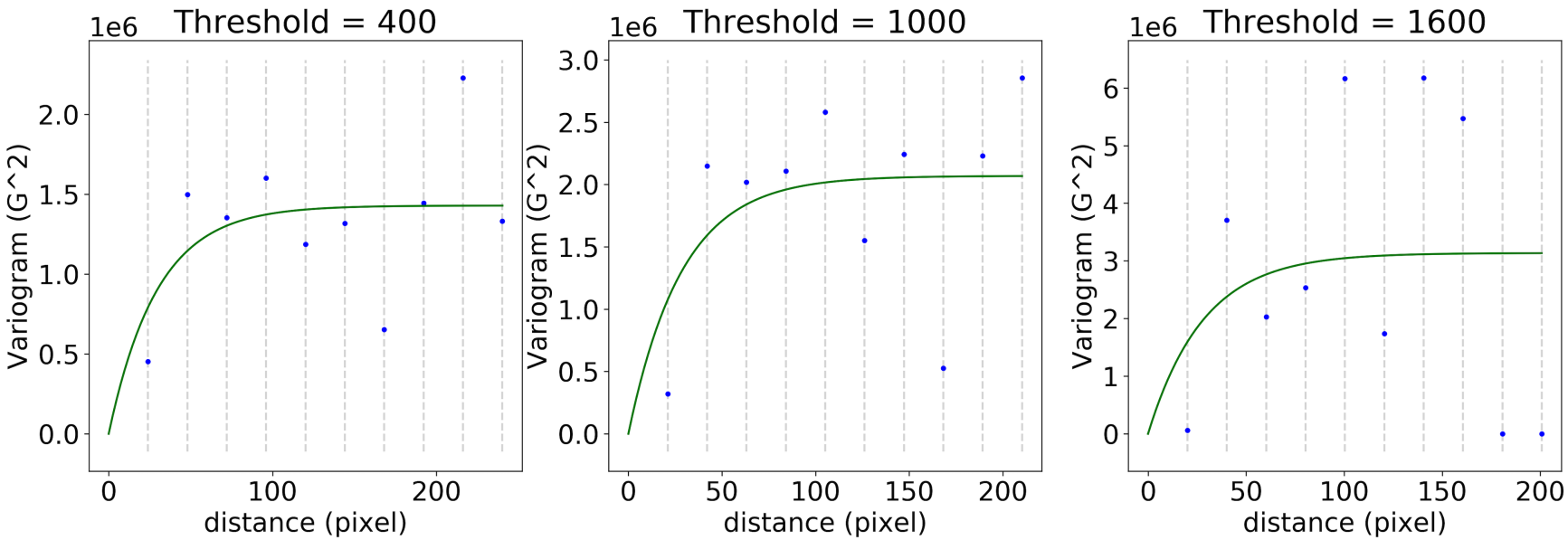

Figure: Variogram examples. Vertical dashed line show the center of each distance interval, and the scatter points are the semi-variance (see equation 1) of B_r values for all pairs of pixels separated by the distance within the interval. The blue line is the fitted curve for the variogram estimates. Note that the scales of x,y axes are different across the three graphs.

Feature Overview

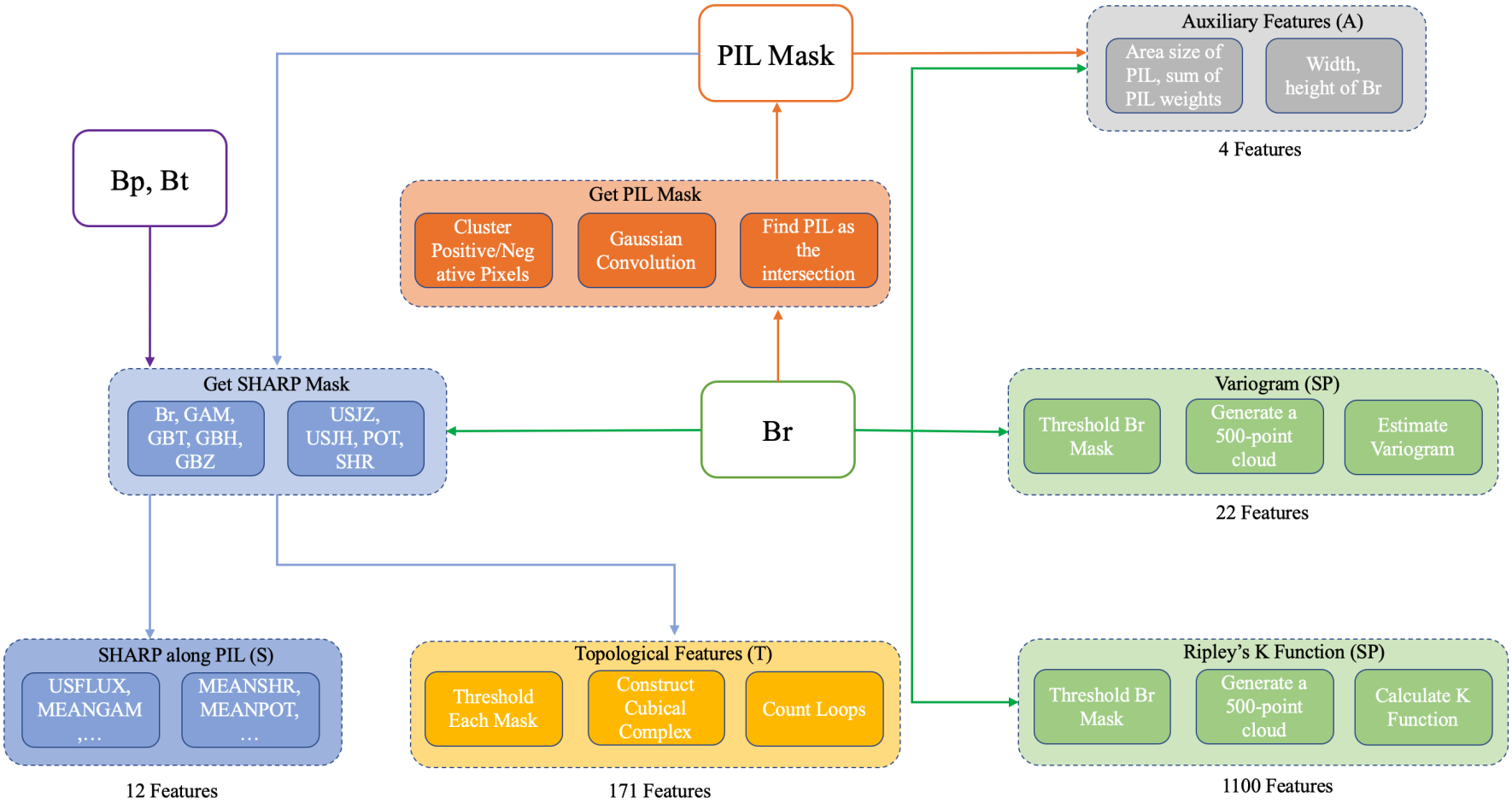

Figure: A Workflow Summary of the Derived Features

True Skill Score based on Fitted Xgboost Model

Feature Combination	1	6	12	24
S	0.496	0.487	0.455	0.390
T	0.487	0.521	**0.507**	**0.473**
SP	0.473	0.482	0.467	**0.459**
S+T	0.520	0.507	**0.495**	**0.491**
S+SP	0.507	**0.508**	**0.472**	**0.451**
S+T+SP	**0.539**	**0.528**	**0.515**	**0.505**
S+T_PC+SP_PC	0.505	0.502	0.483	**0.457**
S+T+SP+A	**0.544**	**0.540**	**0.515**	**0.505**
S+T_PC+SP_PC+A	0.510	0.505	**0.487**	**0.453**

Feature Importance: Fisher Score

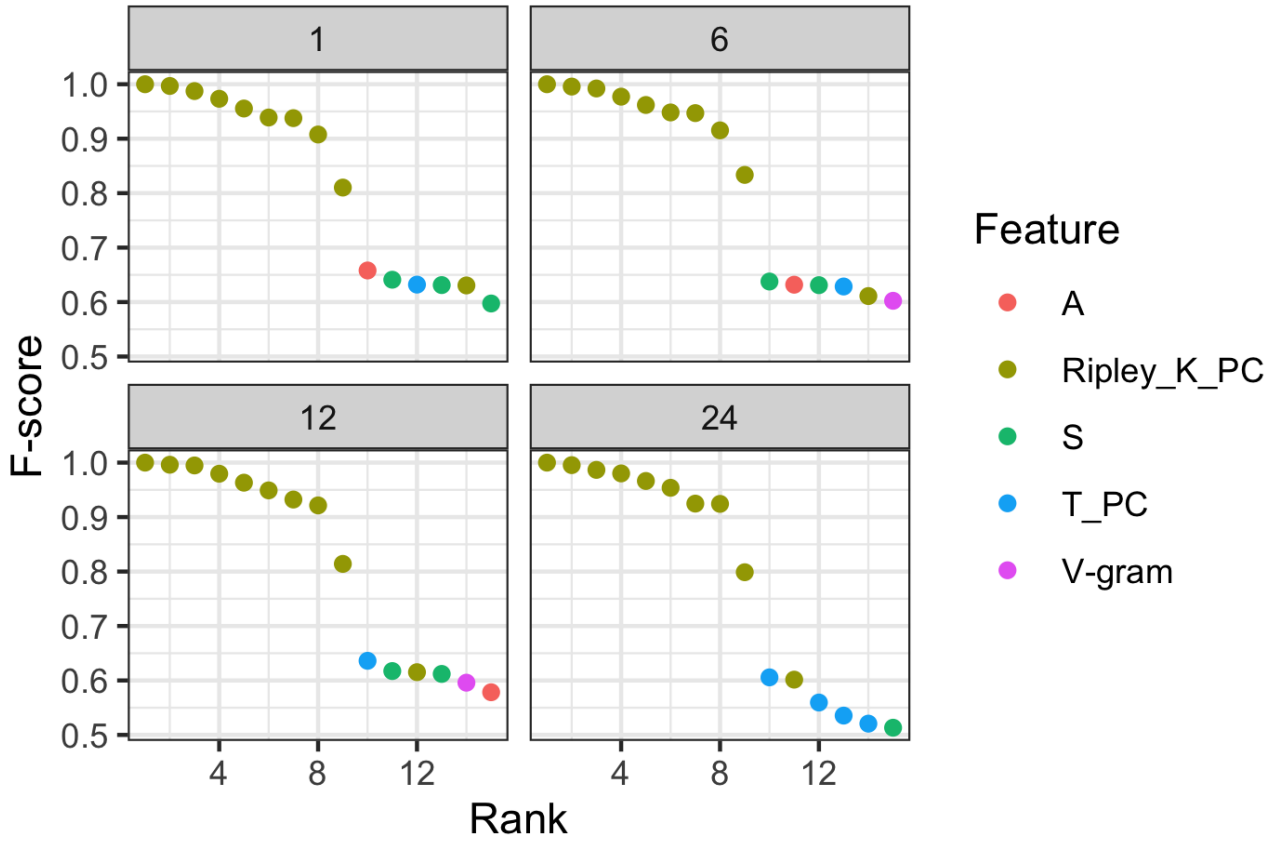

Figure: Normalized Fisher Score for selected features. Four panels correspond to the 1,6,12,24 hour dataset. Among all 4 datasets, the top features are always the Ripley's K function's principal component score. Some features from other categories are also ranked among top features.

Ripley's K function: B-flare Example

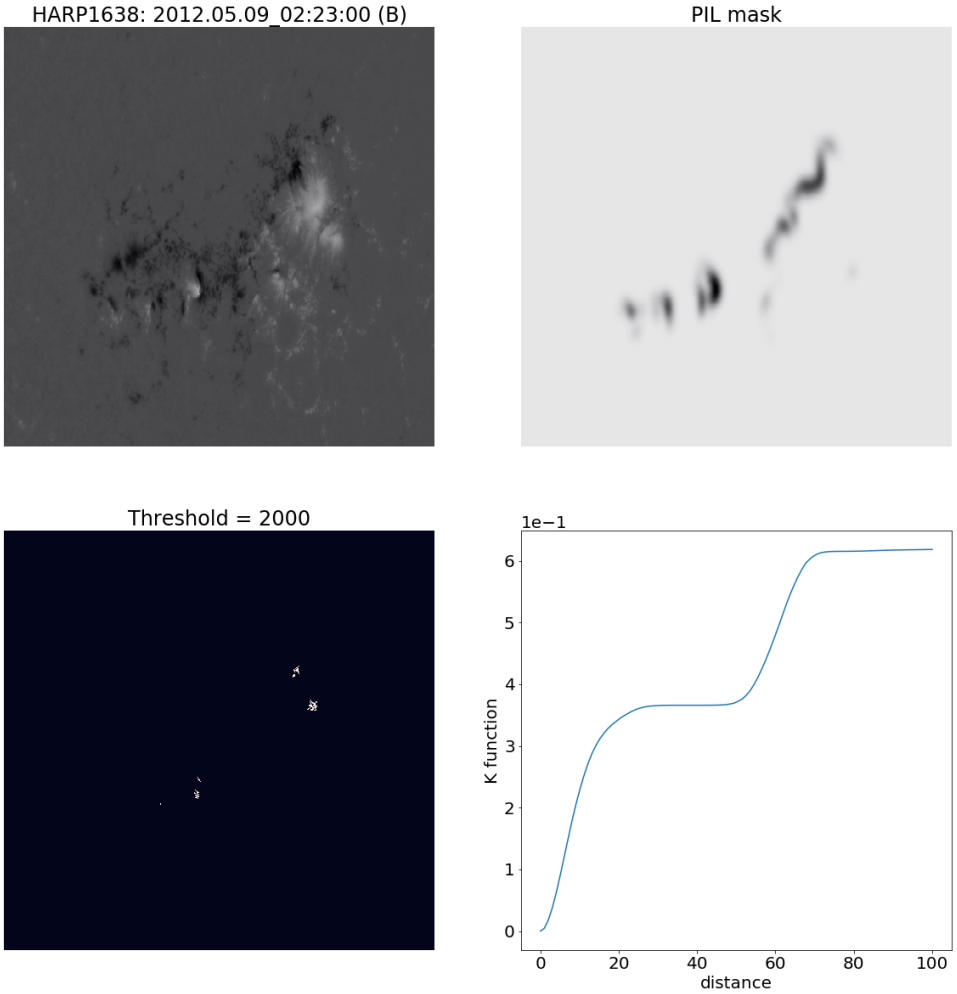

Ripley's K function: M-flare Example

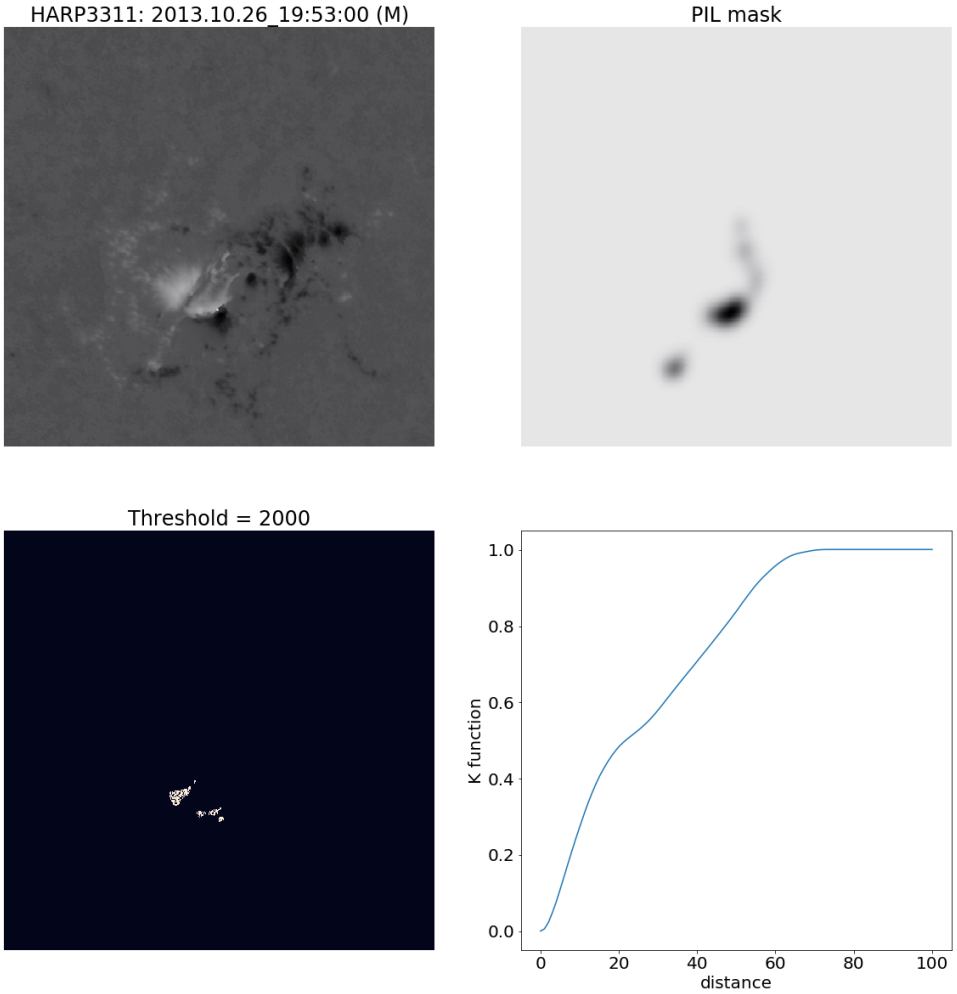

Conclusion

In this project, we:

- Concentrate on SHARP parameter spatial distributions along the polarity inversion line regions.

Conclusion

In this project, we:

- Concentrate on SHARP parameter spatial distributions along the polarity inversion line regions.
- Engineered interpretable and predictive features summarizing the spatial variation, dispersion patterns of various SHARP quantities, especially the B_r, using tools from TDA and spatial statistics.

Conclusion

In this project, we:

- Concentrate on SHARP parameter spatial distributions along the polarity inversion line regions.
- Engineered interpretable and predictive features summarizing the spatial variation, dispersion patterns of various SHARP quantities, especially the B_r, using tools from TDA and spatial statistics.
- Obtained marginal but steady improvement on the solar flare classification task.

Conclusion

In this project, we:

- Concentrate on SHARP parameter spatial distributions along the polarity inversion line regions.
- Engineered interpretable and predictive features summarizing the spatial variation, dispersion patterns of various SHARP quantities, especially the B_r, using tools from TDA and spatial statistics.
- Obtained marginal but steady improvement on the solar flare classification task.
- Reveal that the B_r channel alone contains flare predictors (based on Spatial statistics) that are as predictive as (or better than) the SHARP parameters, which are based on more magnetic field channels.

References I

Bobra, M. G., X. Sun, J. T. Hoeksema, M. Turmon, Y. Liu, K. Hayashi, G. Barnes, and K. D. Leka (Sept. 2014). "The Helioseismic and Magnetic Imager (HMI) Vector Magnetic Field Pipeline: SHARPs – Space-Weather HMI Active Region Patches". In: *Solar Physics* 289.9, pp. 3549–3578.

Bobra, Monica G and Sebastien Couvidat (2015). "Solar flare prediction using SDO/HMI vector magnetic field data with a machine-learning algorithm". In: *The Astrophysical Journal* 798.2, p. 135.

Camporeale, Enrico (July 2019). "The Challenge of Machine Learning in Space Weather Nowcasting and Forecasting". In: *Space Weather* 17. DOI: 10.1029/2018sw002061.

References II

Chen, Yang, Ward B Manchester, Alfred O Hero, Gabor Toth, Benoit DuFumier, Tian Zhou, Xiantong Wang, Haonan Zhu, Zeyu Sun, and Tamas I Gombosi (2019). "Identifying solar flare precursors using time series of SDO/HMI Images and SHARP Parameters". In: *Space Weather* 17.10, pp. 1404–1426.

Deshmukh, Varad, Thomas Berger, James Meiss, and Elizabeth Bradley (2020). "Shape-based Feature Engineering for Solar Flare Prediction". In: *arXiv preprint arXiv:2012.14405*.

Deshmukh, Varad, Thomas E Berger, Elizabeth Bradley, and James D Meiss (2020). "Leveraging the mathematics of shape for solar magnetic eruption prediction". In: *Journal of Space Weather and Space Climate* 10, p. 13.

References III

Florios, Kostas, Ioannis Kontogiannis, Sung-Hong Park, Jordan A Guerra, Federico Benvenuto, D Shaun Bloomfield, and Manolis K Georgoulis (2018). "Forecasting Solar Flares Using Magnetogram-based Predictors and Machine Learning". In: *Solar Physics* 293.2, p. 28. DOI: doi:10.1007/s11207-018-1250-4.

Jiao, Zhenbang, Hu Sun, Xiantong Wang, Ward Manchester, Tamas Gombosi, Alfred Hero, and Yang Chen (2020). "Solar flare intensity prediction with machine learning models". In: *Space Weather* 18.7, e2020SW002440.

Liu, Hao, Chang Liu, Jason T. L. Wang, and Haimin Wang (June 2019). "Predicting Solar Flares Using a Long Short-term Memory Network". In: *The Astrophysical Journal* 877.2, p. 121. DOI: 10.3847/1538-4357/ab1b3c. URL: https://doi.org/10.3847%2F1538-4357%2Fab1b3c.